protonated and deprotonated species coexist as equilibrium mixtures (eq 1) in aqueous micellar solutions at pH lower than 10. The equilibrium of eq 1, however, lies far to the right at pH higher than 10, resulting in the redox potential being almost constant. The pK values of the clusters obtained from the redox potential nature of the surface-active agents used to form micellar solutions have little effect on the pK values of the clusters. The pK values of the clusters may reflect not only the hydrophobicity of the environment of the cluster but also the basicity of the Fe_4S_4 cores.[31] The present clusters have pK values somewhat larger than those of iron-sulfur proteins reported so far (pK = 6.5-8.9).[28,31-33] A most possible site for the protonation of **1**, **2**, or **3** is a terminal[34] or a bridged sulfur atom, since both atoms in some high-potential iron-sulfur proteins are basic enough to form stable hydrogen bondings with the NH proton of polypeptide chains.[20-22]

Registry No. **1**, 88510-46-7; **2**, 100165-84-2; **3**, 100165-86-4; $(Et_4N)_3[Mo_2Fe_6S_8(SEt)_9]$, 72895-02-4; HSC_6H_4-*p*-*n*-C_8H_{17}, 4527-48-4; Triton X-100, 9002-93-1; potassium *p*-octylbenzenesulfonate, 73948-22-8; dodecyltrimethylammonium chloride, 112-00-5.

(31) Magliozzo, R. S.; McIntosh, B. A.; Sweeney, W. V. *J. Biol. Chem.* **1982**, *257*, 3506.

(32) Knaff, D. B.; Malkin, R. *Arch. Biochem. Biophys.* **1973**, *159*, 555.
(33) Malkin, R.; Bearden, A. J. *Biochim. Biophys. Acta* **1978**, 505, 147.
(34) The pK value of HSC_6H_4-*p*-*n*-C_8H_{17} determined by potentiometric titration in an aqueous Triton X-100 solution at 30 °C is 10.87.

Contribution from the Departments of Chemistry, Canisius College, Buffalo, New York 14208, and University of Bern, CH-3000 Bern 9, Switzerland

Optical Spectra of Exchange-Coupled Manganese(II) Pairs in Cadmium Chloride and Cadmium Bromide

Paul J. McCarthy*[1a] and Hans U. Güdel[1b]

Received July 25, 1985

The high-resolution optical absorption spectra of $Cd_{0.92}Mn_{0.08}Cl_2$ and $Cd_{0.85}Mn_{0.15}Br_2$ show clear evidence of manganese(II) pair exchange interactions in the $^4A_1{}^4E(G)$, $^4T_2(D)$, and $^4E(D)$ regions of the spectra. From the variation of band intensities between 1.4 and 3.0 K, values of J = 1.43 and 1.33 cm^{-1} were determined for the ground-state exchange parameter in $Mn_2Cl_{10}^{6-}$ and $Mn_2Br_{10}^{6-}$, respectively. These values provide a good estimate of nearest-neighbor exchange interactions in pure manganese(II) chloride and manganese(II) bromide. The effective exchange parameter in the excited $^4A_1(G)$ state is approximately 30% larger than J in both dimers.

Introduction

The study of excited states of coupled dimers provides deeper insight into the nature and mechanisms of exchange interactions than the study of ground-state properties alone.[2] Recent optical[3] and inelastic neutron-scattering[4] work on the chain compounds $CsMg_{1-x}Mn_xBr_3$ shows that the interaction in isolated $Mn_2Br_9^{5-}$ dimers is a very good measure of the nearest-neighbor exchange in pure $CsMnBr_3$. Mn(II) compounds with layer structures, such as manganese(II) chloride and manganese(II) bromide, are not as well characterized. Transitions to very complicated 3D magnetically ordered phases were observed at 1.96 and 1.81 K for manganese(II) chloride and at 2.30 K for manganese(II) bromide.[5,6] For these compounds, however, no estimates of nearest-neighbor exchange constants are available. Detailed spectroscopic and magneto-optical studies have been reported for the pure compounds, manganese(II) chloride[6] and manganese(II) bromide.[7,8] Dominant effects due to the magnetic coupling were observed at low temperatures. Very little, on the other hand, has been reported on the analogous diluted systems. While some evidence for dimer absorptions in $Cd_{0.85}Mn_{0.15}Cl_2$ was noted by Trutia et al.,[9] they made no thorough study down to very low temperatures, where the magnetic effects are expected to become dominant. We therefore decided to study the diluted systems $Cd_{1-x}Mn_xCl_2$ and $Cd_{1-x}Mn_xBr_2$ in order to determine exchange splittings and exchange parameters in the $Mn_2Cl_{10}^{6-}$ and $Mn_2Br_{10}^{6-}$ dimers.

Experimental Section

Crystal Preparation. The Bridgman technique was used to prepare cadmium chloride and cadmium bromide doped with 8 and 15 mol % manganese. Two of the four crystals prepared were of superior optical quality and were used almost exclusively for the spectroscopic investigations.

Crystal Structures. Cadmium chloride, cadmium bromide, and manganese(II) chloride are isomorphous and belong to space group $D_{3d}^5(R\bar{3}m)$.[10] The structures contain a cubic close packing of the anions.[11] Manganese(II) bromide belongs to space group $D_{3d}^3(P\bar{3}m1)$ and has hexagonal close-packed layers.[12] Since all these structures contain sheets of edge-sharing MX_6 octahedra, the crystals cleave very readily perpendicular to the threefold axis to yield samples that can be used without further polishing to obtain axial spectra. For the σ ($E \perp c$) and π ($E \parallel c$) spectra the crystals must be cut and polished parallel to the unique axis, a somewhat more troublesome procedure.

Spectroscopic Measurements. Some absorption spectra were obtained on a Cary 17 spectrophotometer equipped with an Air Products closed-cycle cryogenic refrigerator. With this apparatus spectra were recorded

(1) (a) Canisius College. (b) University of Bern.
(2) Güdel, H. U. "Magneto-Structural Correlations in Exchange Coupled Systems"; D. Reidel Publishing Co.: Dordrecht, The Netherlands, 1985; pp 297-327.
(3) McCarthy, P. J.; Güdel, H. U. *Inorg. Chem.* **1984**, *23*, 880.
(4) Falk, U.; Furrer, A.; Kjems, J. K.; Güdel, H. U. *Phys. Rev. Lett.* **1984**, *52*, 1336.
(5) Regis, M.; Farge, Y.; Royce, B. S. H. *AIP Conf. Proc.* **1976**, *29*, 654 and ref 1 and 2 therein.
(6) Regis, M.; Farge, Y. *J. Phys.* (*Les Ulis, Fr.*) **1976**, *37*, 627.
(7) Hoekstra, H. J. W. M.; Folkersma, H. F.; Haas, C. *Solid State Commun.* **1984**, *51*, 657.
(8) Farge, Y.; Regis, M.; Royce, B. S. H. *J. Phys.* (*Les Ulis, Fr.*) **1976**, *37*, 637.
(9) Trutia, A.; Ghiordanescu, V.; Voda, M. *Phys. Status Solidi B* **1975**, *70*, K19.
(10) Wycoff, R. W. G. "Crystal Structures", 2nd ed.; Interscience: New York, 1965; Vol. 1, p 270 ff.
(11) Ferrari, A.; Braibanti, A.; Bigliardi, G. *Acta Crystallogr.* **1963**, *16*, 846.
(12) Wollan, E. O.; Koehler, W. C.; Wilkinson, M. K. *Phys. Rev.* **1958**, *110*, 638.

0020-1669/85/1325-0838$01.50/0 © 1986 American Chemical Society

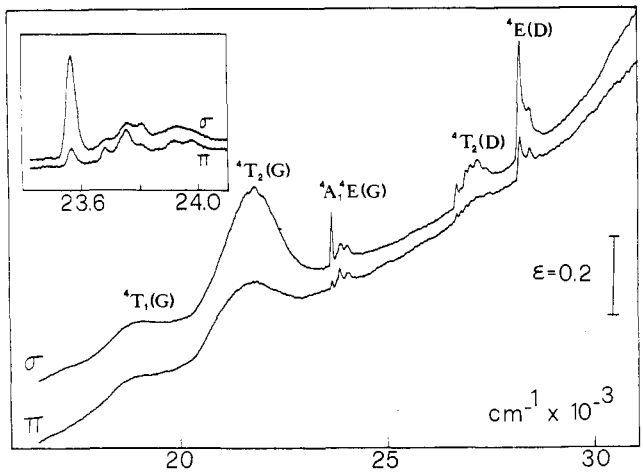

Figure 1. Single-crystal absorption spectra of $Cd_{0.92}Mn_{0.08}Cl_2$ at 13 K. Octahedral labels are used although the actual symmetry is trigonal. Inset: $^4A_1{}^4E(G)$ region.

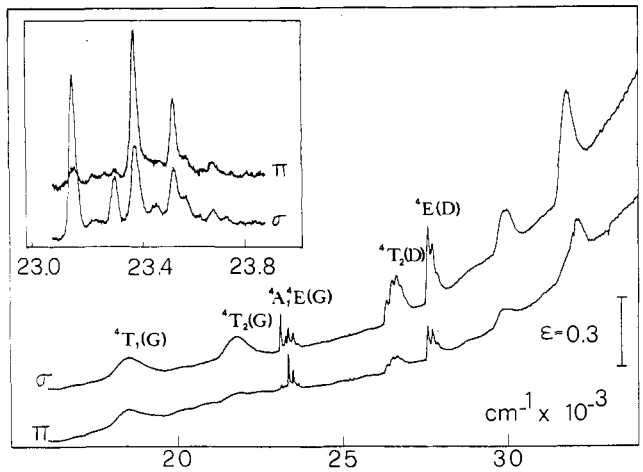

Figure 2. Single-crystal absorption spectra of $Cd_{0.85}Mn_{0.15}Br_2$ at 13 K. Octahedral labels are used although the actual symmetry is trigonal. Inset: $^4A_1{}^4E(G)$ region.

down to about 13 K. A pair of Glan–Taylor prisms were used to obtain plane-polarized light.

High-resolution spectra were made by dispersing the light of a halogen lamp with a $^3/_4$-m monochromator (Spex 1702). Samples were cooled in an Oxford Instruments SM4 cryomagnet, with which temperatures down to 1.4 K were attained. Detection was made with a cooled photomultiplier tube (RCA 31034) using a chopper and a lock-in amplifier (PAR 186A).

Results

Overall Spectra. Figures 1 and 2 show the spectra of $Cd_{0.92}Mn_{0.08}Cl_2$ and $Cd_{0.85}Mn_{0.15}Br_2$ at 13 K. Since the spectra of pure manganese(II) chloride and bromide have been extensively studied,[6-8,13-17] the principal band assignments in the mixed crystals up to and including $^4E(D)$ are straightforward. Octahedral labels are used for convenience even though the chromophore in each is trigonally distorted.

Axial spectra recorded under conditions similar to those in Figures 1 and 2 clearly show the equivalence of the σ and axial spectra. The spectra are thus electric dipolar (ED).

In the spectra of the chloride compound we were able to observe no bands beyond those shown in Figure 1. Besides the features clearly seen in Figure 1 and in the other figures in this paper, we may note that in σ polarization the second band, $^4T_2(G)$, shows a short progression in ca. 213 cm^{-1}, the totally symmetric Mn–Cl stretching frequency. The room-temperature Raman spectrum of manganese(II) chloride yields a value of 234 cm^{-1} for the a_1 mode.[18]

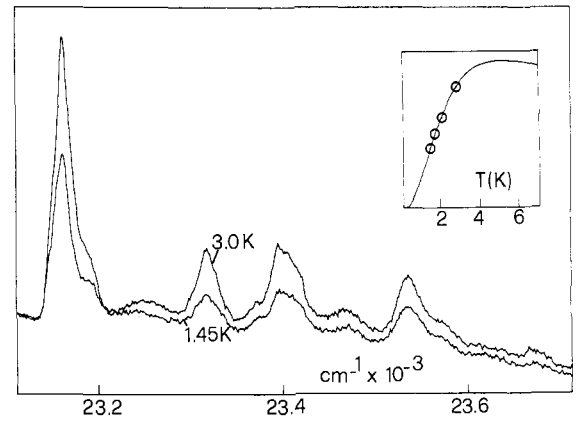

Figure 3. Temperature dependence of the axial spectrum of the $^4A_1{}^4E(G)$ band of $Cd_{0.85}Mn_{0.15}Br_2$. Inset: observed band areas below 3 K and Boltzmann populations calculated with $J = 1.33$ cm^{-1} (see text).

In the bromide spectra four bands higher in energy than the $^4E(D)$ were seen: (1) a broad weak band of uncertain origin at about 29 100 cm^{-1} (barely seen in Figure 2); (2) a strong band at 30 000 cm^{-1} which decreases markedly in intensity and develops some weak structure as the crystal is cooled to 13 K, probably the $^4T_1(P)$ state; (3) a strong band of uncertain origin at about 31 900 cm^{-1} (since its relative intensity at 13 K varies in different crystals, it should not be assigned to the same species that produces the rest of the spectrum); (4) a band (not shown in Figure 2) in the axial spectrum of $Cd_{0.85}Mn_{0.15}Br_2$ beginning at 34 692 cm^{-1}, which consists of a five-membered progression in 141 ± 2 cm^{-1}, the totally symmetric Mn–Br stretching frequency (ground-state value 151 cm^{-1}).[16] Band 4 has been assigned to the $^4A_2(F)$ state in manganese(II) bromide by Pollini et al.[16]

The absorptions in these spectra are in general 1 order of magnitude more intense than those of isolated Mn^{2+} ions in a similar environment. This is in agreement with their ED character and is a clear manifestation of exchange interactions between the coupled Mn^{2+} ions. This exchange intensity mechanism has been treated by many authors[19] and will be discussed for the present dimers in the next section.

Comparison of the overall axial spectra of $Cd_{0.92}Mn_{0.08}Cl_2$ and $Cd_{0.85}Mn_{0.15}Cl_2$ shows that with increased manganese concentration intensity enhancement is very noticeable in the $^4A_1{}^4E(G)$, $^4T_2(D)$, and $^4E(D)$ bands. These bands were accordingly studied at very low temperatures in the hope of finding in their temperature dependence indications of manganese pair (and larger cluster) interactions.

$^4A_1{}^4E(G)$ Region. The insets in Figures 1 and 2 show this region for the two crystals at 13 K. The spectra of the two compounds are similar in general contour and also with regard to polarization of the bands. In particular, the lowest energy band in both is almost completely σ-polarized, and another band 187 cm^{-1} to higher energy in the chloride and 223 cm^{-1} in the bromide is strongly π-polarized. In each spectrum these two bands may be the electronic origins for the $^4A_1(G)$ and $^4E(G)$ states. The ordering of the states is not, however, certain. Calculations on manganese(II) bromide have placed $^4A_1$ lower than ^4E,[14] but no firm assignments could be made on the basis of single-crystal experiments.[16]

The vibrational fine structure is better resolved in the bromide than in the chloride. The prominent sidebands are approximately 150 and 230 cm^{-1}, respectively, displaced from the electronic origins. They correspond to the totally symmetric Mn–X

(13) Pappalardo, R. *J. Chem. Phys.* **1959**, *31*, 1050.
(14) Stout, J. W. *J. Chem. Phys.* **1960**, *33*, 303.
(15) Low, W.; Rosengarten, G. *J. Mol. Spectrosc.* **1964**, *12*, 319.
(16) Pollini, I.; Spinolo, G.; Benedek, G. *Phys. Rev. B: Condens. Matter* **1980**, *22*, 6369.
(17) Ghosh, B.; Mukherjee, R. K. *Phys. Status Solidi B* **1980**, *102*, K89.
(18) Lockwood, D. J. *J. Opt. Soc. Am.* **1973**, *63*, 374.
(19) Ferguson, J. *Prog. Inorg. Chem.* **1970**, *12*, 159.

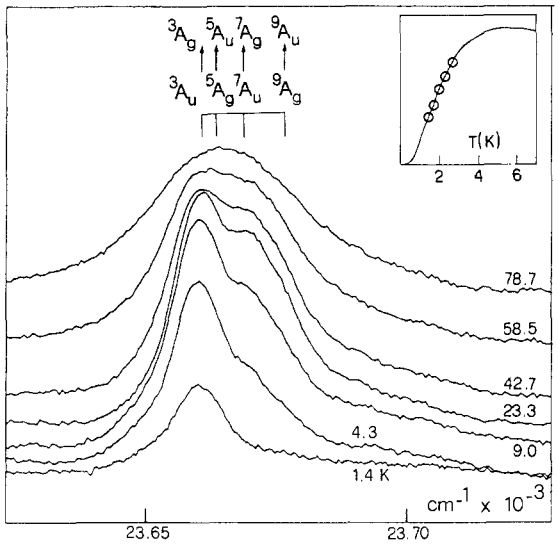

Figure 4. Temperature dependence of the axial spectrum of the lowest energy band in the $^4A_1{}^4E(G)$ region of $Cd_{0.92}Mn_{0.08}Cl_2$. Inset: observed band areas below 3 K and Boltzmann populations calculated with J = 1.43 cm^{-1} (see text).

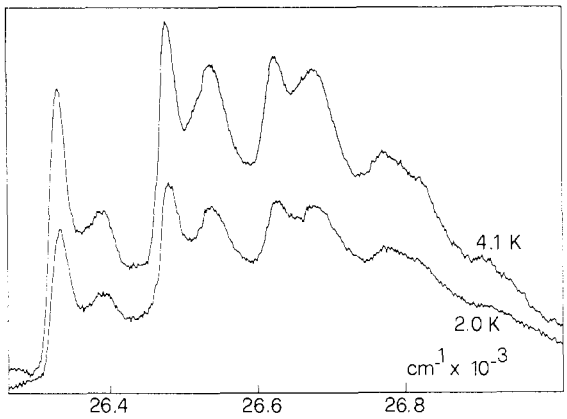

Figure 5. Temperature dependence of the axial spectrum of the $^4T_2(D)$ band of $Cd_{0.85}Mn_{0.15}Br_2$.

stretching frequencies, which were found at 151 and 234 cm^{-1} in pure manganese(II) bromide and chloride by Raman spectroscopy.[16] The remaining structure is not intense, and we conclude that there is only a minor contribution to the $^4A_1{}^4E(G)$ intensity from a vibronic mechanism. This is in good agreement with the dominance of an exchange intensity mechanism discussed below.

All the major bands in the $^4A_1{}^4E(G)$ region show the same temperature dependence. As illustrated for the bromide system in Figure 3, the decrease in intensity on lowering the temperature from 3.0 to 1.5 K is very pronounced. This clearly shows that all the bands are exchange-induced (see the Discussion). From their concentration dependence we can further deduce that they are all dimer bands. Single manganese centers may contribute to the intensity at higher temperatures by way of a vibronic mechanism. Above 50 K the bands are too broad, however, to separate the various contributions.

Figure 4 shows the temperature dependence of the principal band at 23 661 cm^{-1} in $Cd_{0.92}Mn_{0.08}Cl_2$. A change of shape is clearly in evidence in addition to the intensity change. There is an overall shift to higher energy with increasing temperature, with a shoulder 8 cm^{-1} above the principal band barely resolved between 4 and 40 K. These effects are due to the dimeric nature of the corresponding transitions and will be discussed in the next section.

The behavior of $Cd_{0.85}Mn_{0.15}Br_2$ is very similar. The principal line at 23 153 cm^{-1} shows some weak shoulders at 1.45 K, which, from their temperature behavior, cannot be dimer transitions. The intensity increase of the 23 153-cm^{-1} dimer band is reproduced in Figure 3 (inset).

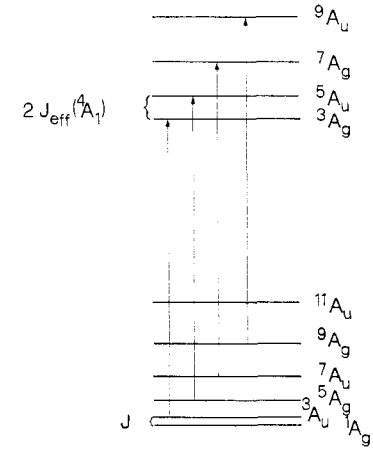

Figure 6. Schematic diagram of $^6A_1 \rightarrow {}^4A_1$ single pair excitations.

Table I. $O \rightarrow C_2$ Correlation for Spectroscopically Relevant Single-Ion States and Polarizations of Pair Transitions (P) with Respect to Crystal c Axis

O	C_2	P
A_1	A	σ
E	A	σ
	B	π
T_1	A	σ
	B	π
	B	π
T_2	A	σ
	A	σ
	B	π

$^4T_2(D)$ Region. The axial spectra of the entire $^4T_2(D)$ band system of $Cd_{0.85}Mn_{0.15}Br_2$ at 2.0 and 4.1 K are shown in Figure 5. The large increase in intensity corresponds to that observed in the $^4A_1{}^4E(G)$ region, and the spectrum is thus identified as a dimer spectrum. It is dominated by two progressions in 147 cm^{-1}, the totally symmetric Mn–Br stretching frequency. The origins, separated by 58 cm^{-1}, correspond to two spin–orbit components of $^4T_2(D)$. At 13 K the axial spectrum shows an additional weak band between the first two bands in Figure 5. The spectrum of pure manganese(II) bromide is also dominated by totally symmetric progressions in this band system.[16]

The $^4T_2(D)$ spectrum of the chloride complex (not shown here) has, within experimental accuracy, the same temperature dependence as the $^4A_1{}^4E(G)$ region and is therefore identified as a dimer spectrum. It has two short totally symmetric progressions in about 225 cm^{-1}, the first members being separated by about 95 cm^{-1}. In contrast to that of the bromide, the first prominent origin is split by 14 cm^{-1} into two components.

$^4E(D)$ Region. This band system in both crystals shows the typical strong temperature dependence below 5 K. It therefore belongs to Mn(II) pairs. As in the case of the pure compounds, manganese(II) chloride and bromide, the dominant feature is progressions in the totally symmetric stretching mode (about 225 cm^{-1} for the chloride and 150 cm^{-1} for the bromide) built on a strong origin. The origin in each crystal consists of at least three partly resolved spin–orbit components; the two principal components in the chloride are separated by 14 cm^{-1}.

Discussion

Pair Energies. Manganese(II) has a spin-only ground state. The exchange interactions can therefore be represented by the Heisenberg Hamiltonian

$$\hat{H} = J(\vec{S}_a \cdot \vec{S}_b) \qquad (1)$$

For an antiferromagnetic interaction J is positive, and the eigenvalues of eq 1 form a Landé splitting pattern as shown in Figure 6. J is the singlet–triplet separation. The symmetry labels of the states refer to the C_{2h} pair point group. They are obtained by correlating the octahedral (O) and C_2 single-ion species (Table I) and then constructing the proper $^6A_1{}^6A_1$ pair wave functions.

Since $^6A_1 \rightarrow {}^4A_1$ (octahedral notation) is an intraconfigurational transition in first order, the exchange coupling in the corresponding singly excited pair states can be represented by[20]

$$\hat{H}' = \sum_{ij} J_{ai,bj}(\vec{s}_{ai}\cdot\vec{s}_{bj}) \quad (2)$$

where i and j number the unpaired electron orbitals on centers a and b, respectively. $J_{ai,bj}$ are orbital exchange parameters. As was shown in ref 2, they can be correlated to $J_{eff}(^4A_1)$ by

$$J_{eff}(^4A_1) = \tfrac{1}{25}[\tfrac{25}{18}\sum J_{tt} + \tfrac{25}{24}\sum J_{ee} + \tfrac{25}{18}\sum J_{te}] \quad (3)$$

Proper pair wave functions are given by

$$\phi_{\pm} = (1/2^{1/2})[|^4A_1{}^6A_1\rangle \pm |^6A_1{}^4A_1\rangle] \quad (4)$$

Spin values range from $S = 1$ to $S = 4$, so that there are a total of eight pair levels. Four of these have the right symmetry to be spectroscopically accessible from the ground-state levels. They form a Landé-type splitting pattern as shown in Figure 6. This diagram can now be used to rationalize the spectra in Figure 4. The marked decrease of intensity on cooling below liquid-helium temperature is the result of a depopulation of those pair ground levels from which allowed transitions to excited states are possible. At 1.4 K this depopulation is not yet complete, but it is a fair guess that the spectrum would vanish completely if we could reach lower temperatures. We can use the observed temperature dependence of intensity at the very lowest temperatures to obtain an estimate of the singlet–triplet separation.

The temperature dependence of the principal band in the $^4A_1{}^4E(G)$ region of $Cd_{0.92}Mn_{0.08}Cl_2$ is shown in Figure 4. The change in band contour with increasing temperature indicates that even at 1.4 K the principal band consists of both $S = 1$ and $S = 2$ transitions; the other two pair transitions first appear at higher temperature. The four transitions are indicated in Figure 4. If the lowest energy band is assumed to be symmetrical with the higher energy side mirroring the contour of the lower energy side, the change in area with temperature yields a value of $J = 1.43$ cm^{-1}. This is the best fit if only the spectra below 3 K are used and if the $S = 1$ and $S = 2$ transitions are weighted with the factors 7 and 30 expected from theory.[20]

A detailed temperature study was carried out only on the first band of this system in the bromide. Even at 1.4 K a shoulder is seen about 32 cm^{-1} above the principal band at 23 153 cm^{-1}. This is most likely not a dimer band, and its area at 1.4 K was measured and subtracted from the overall band areas at all temperatures. This gave an estimate of the area of the first band, which, as in the case of the chloride, we assigned to the $S = 1$ plus $S = 2$ transitions. Above 2.1 K a shoulder 9 cm^{-1} higher in energy began to be seen. This we associate with the other two pair transitions. Use of the same procedure as in the case of the chloride yielded a value of $J = 1.33$ cm^{-1}.

These values of J are a good estimate of the nearest-neighbor intralayer exchange parameters in pure manganese(II) chloride and bromide. Values for this interaction have not been previously reported. It is clear that J is smaller for the bromide than for the chloride, as was found also for the complexes $CsMg_{1-x}Mn_xX_3$ (X = Cl, Br; $x = 0.04$–0.20).[3] It is also the trend we would expect for kinetic exchange,[21] because the relevant electron-transfer integrals are smaller in the bromide than in the chloride.

The insets in Figures 3 and 4 show calculated and experimental values. At temperatures above 2 K there is appreciable population of the $S = 2$–5 ground levels. In addition to changes in intensity this also leads to the observed energy shift in Figure 4. The shift is toward higher energies with increasing temperature. We conclude that $J_{eff}(^4A_1)$ must be larger than J by approximately 1.0 cm^{-1} in $Mn_2Cl_{10}^{6-}$ and 0.9 cm^{-1} in $Mn_2Br_{10}^{6-}$. An increase of about 30% in the exchange parameter between the $^6A_1{}^6A_1$ ground state and the $^6A_1{}^4A_1$ excited state has also been found in other Mn(II) dimers.[3,22]

In order to make some estimates about the orbital parameters, we need the correlation between the orbital parameters and J for the ground state:

$$J = \tfrac{1}{25}[\sum J_{tt} + 2\sum J_{te} + \sum J_{ee}] \quad (5)$$

Assuming the orbital parameters to have the same values in the ground and excited state, we conclude from eq 3 and 5 and the experimental J and $J_{eff}(^4A_1)$ values that $\sum J_{tt}$ must be the dominant antiferromagnetic term. If there were no contribution from $\sum J_{te}$ and $\sum J_{ee}$, we would expect a $J_{eff}(^4A_1)/J$ ratio of 1.4. The experimental ratio of 1.7 is in reasonable agreement with this. But the following must also be considered. Despite the fact that $^6A_1 \rightarrow {}^4A_1$ transitions take place within a given electron configuration in first order, there is some experimental evidence that reality deviates slightly from this idealization. The electronic origin is the dominant band in the absorption spectrum, but a significant fraction lies in the members of a totally symmetric progression (see Figure 3). The potential surfaces reflecting the chemical bonding in the two states are slightly different. The orbital exchange parameters may therefore also be somewhat different in the two states. If $J_{eff}(^4A_1)$ is larger than J by 30–40%, then $\sum J_{ee}$ could be the leading antiferromagnetic term. $\sum J_{te}$ can under no circumstances be a dominant antiferromagnetic term, as expected theoretically.

It is interesting to compare the edge-sharing nearest-neighbor $Mn_2X_{10}^{6-}$ dimers in the layer compounds $Cd_{1-x}Mn_xX_2$ with the corresponding face-sharing $Mn_2X_9^{5-}$ dimers in the chain compounds $CsMg_{1-x}Mn_xX_3$. J values are 1 order of magnitude larger in the latter. This can be rationalized in terms of orbital exchange parameters. One-electron orbitals are trigonally quantized in both classes of compounds. As was noted in ref 3, $J_{t^0t^0}$ is a good candidate for a dominant antiferromagnetic contribution in $Mn_2X_9^{5-}$. The t^0 trigonal orbitals of nearest neighbors in the chain are pointing directly toward each other. As a consequence we expect the corresponding one-electron-transfer integral and thus the kinetic exchange contribution to $J_{t^0t^0}$ to be dominant. These ideas are fully supported by the much smaller exchange parameters determined for $Mn_2X_{10}^{6-}$ in this study. The disposition of t^0 orbitals on nearest neighbors is such that there is no overlap, and accordingly, $J_{t^0t^0}$ is not expected to contribute.

Polarizations and Intensities. Pair transitions can get ED intensity from a single-ion or an exchange mechanism.[23] The former makes use of the odd-parity crystal field at the manganese site in conjunction with spin–orbit coupling. It is the same mechanism that provides intensity for spin-forbidden transitions in monomeric complexes. The exchange mechanism was first proposed by Tanabe.[20] It can provide intensity for spin-forbidden (in the single ion) transitions in dimers, higher clusters, and extended magnetic systems. For the case of our Mn(II) dimers the exchange mechanism leads to the selection rules $\Delta S = 0$ and $\Delta M_S = 0$, where S and M_S are dimer quantum numbers. With a single-ion mechanism, on the other hand, transitions with $\Delta S = \pm 1$ are allowed as well as those with $\Delta S = 0$. These selection rules have a strict meaning, of course, only for transitions between states for which S is a good quantum number. Besides the ground state $^6A_1$, the excited states $^4A_1$ and ^4E (octahderal notation) are such. In the orbital triplets, on the other hand, there is first-order spin–orbit coupling, and S is not as sharply defined. Our experimental data show, however, that even for $^4T_2{}^b$ it is a good approximation to consider S as the relevant quantum number (vide infra).

Symmetry selection rules for the exchange mechanism are easily obtained by considering the symmetry species of the pair states and deriving the usual ED selection rules. An example is shown in Figure 6 for the $^4A_1$ single excitations. The four arrows are the transitions allowed by the Tanabe mechanism. They are all z polarized in C_{2h}. Since the twofold axis of the dimers lies in the hexagonal crystal plane, they are σ-polarized. For the sin-

(20) Ferguson, J.; Guggenheim, H. J.; Tanabe, Y. *J. Phys. Soc. Jpn.* **1966**, *21*, 692.
(21) Anderson P. W. *Solid State Phys.* **1963**, *14*, 99.
(22) Ferguson, J.; Güdel, H. U.; Krausz, E. R.; Guggenheim, H. J. *Mol. Phys.* **1974**, *28*, 893.
(23) Naito, M. *J. Phys. Soc. Jpn.* **1973**, *34*, 1491.

gle-ion mechanism the relevant point group is that at the Mn center, namely, C_2. A quick inspection shows that for pair transitions this leads to the same orbital selection rules as the exchange mechanism. These rules are collected in Table I.

Beside these purely qualitative arguments, we get some quantitative ideas about relative intensities by considering their physical origins. The main source of intensity for the single-ion mechanism is the parity-allowed transitions in the UV region, namely, ligand-to-metal charge-transfer transitions and metal-centered d-p transitions. Both of these sources are expected to lead to a fairly isotropic intensity distribution, because the centers are very close to octahedral. In the Tanabe mechanism ligand-to-metal as well as high-lying metal-to-metal transitions can contribute to the intensity of pair transitions. Whereas the former should lead to a more or less isotropic transition moment, the latter are restricted to the hexagonal plane and should contribute only to the σ intensity.

The overall spectra in Figures 1 and 2 show a predominance of σ intensity in the whole spectral range. $^4T_1(G)$ in the chloride host is the only band with comparable intensity in σ and π. This dominance in σ, together with the absolute intensity of the bands (approximately 1 order of magnitude more intense than in mononuclear Mn(II) complexes), is a clear indication of a dominant exchange mechanism.

Further support for this comes from the observed drastic intensity decrease of *all the band systems* when the crystals are cooled below 4 K. The relative populations of the singlet and triplet dimer levels show the largest variations in this temperature range. In the $^4A_1{}^4E$ region, a satisfactory analysis of the data is possible by assuming that there is no singlet intensity. The behaviors in the $^4T_2(D)$ and $^4E(D)$ regions are similar. We conclude therefore that the exchange mechanism dominates the spectrum.

Acknowledgment. We thank Naomi Furer for preparing the crystals used in this study. P.J.M. is also grateful for support from a Canisius College Summer Faculty Fellowship. Financial support by the Swiss National Science Foundation is acknowledged.

Contribution from The Institute for Cancer Research, Philadelphia, Pennsylvania 19111, and Department of Chemistry, Columbia University, New York, New York 10027

Crystal and Molecular Structure of a Chiral-Specific DNA-Binding Agent: Tris(4,7-diphenyl-1,10-phenanthroline)ruthenium(II)

Barry M. Goldstein,† Jacqueline K. Barton,‡ and Helen M. Berman*

Received July 23, 1985

The crystal and molecular structure of the cationic coordination complex tris(4,7-diphenyl-1,10-phenanthroline)ruthenium(II), $Ru(DIP)_3^{2+}$, has been determined. The complex crystallizes in the monoclinic space group $P2_1/c$ with cell dimensions a = 13.085 (2) Å, b = 24.173 (1) Å, c = 22.773 (4) Å, β = 110.91 (1)°, and Z = 4. The final R value is 0.082. All the phenyl groups are skew to the phenanthroline ligands. There are no stacking interactions in the crystal. A plausible model for the Δ enantiomer binding to right-handed DNA is proposed.

Introduction

The cationic coordination complex tris(4,7-diphenyl-1,10-phenanthroline)ruthenium(II), $Ru(DIP)_3^{2+}$, shows chiral discrimination in binding to different forms of DNA.[1] The Ru-

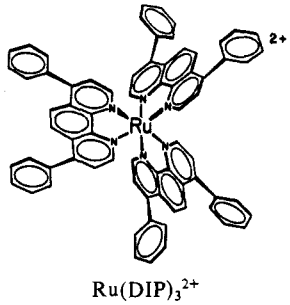

$Ru(DIP)_3^{2+}$

$(DIP)_3^{2+}$ complex possesses both Δ and λ enantiomers due to the asymmetric center at the six-coordinate ruthenium atom. Spectrophotometric studies have shown that both the Δ and λ isomers bind to left-handed Z-DNA.[1a] However, only the Δ enantiomer binds to right-handed B-DNA.[1b] Hence, the stereospecific preferential binding of the λ isomer to Z-DNA provides a molecular probe to distinguish between left- and right-handed DNA helices.[1c]

The development of new chiral probes for DNA that are conformation- and site-specific requires detailed structural information about the metal complexes. As part of an effort to model the binding of $Ru(DIP)_3^{2+}$ to DNA, the structure of the $Ru(DIP)_3^{2+}$ complex has been determined with use of single-crystal X-ray diffraction techniques. On the basis of the structure described here, a more chemically sound model for the binding of $Ru(DIP)_3^{2+}$ to the DNA helix may be considered.

Experimental Section

X-ray Data Collection. Racemic $Ru(DIP)_3^{2+}$ dichloride, $Ru[(C_{12}N_2H_6)(C_6H_5)_2]_3Cl_2$ was obtained as described by Lin et al.[2] A single large red plate (0.5 mm × 0.35 mm × 0.10 mm) was grown by very slow evaporation of a 10 mM solution of the racemic complex in a 24% water/76% methanol (v/v) mixture at 4 °C. The crystal was mounted in a 0.7-mm glass capillary tube containing a strip of filter paper saturated with mother liquor. A preliminary rapid data scan by diffractometer revealed a monoclinic crystal system. The only observed systematic absences were $0k0$ for $k = 2n + 1$ and $h0l$ for $l = 2n + 1$, indicating unambiguously space group $P2_1/c$. Cell dimension and intensity data were collected at 4 °C with use of an Enraf-Nonius CAD-4 diffractometer equipped with a locally designed cooling device[3] and graphite-monochromatized Cu Kα radiation. Lattice constants were obtained by least-squares refinement of the angular settings of 25 reflections in the range θ = 25-30°. The resulting values are a = 13.085 (2) Å, b = 24.173 (1) Å, c = 22.773 (4) Å, β = 110.91 (1)°, and Z = 4. Reflections were measured in the quadrant $(\pm h,-k,l)$ with use of the ω-2θ scan method with a variable scan width $\Delta\omega = (1.75 + 0.15 \tan\theta)°$, this angle being extended 25% on each side for background measurements. The scan rate varied between 1.0 and 4.0° min^{-1} depending upon the value of $\sigma(I)/I$ for each reflection. Data were collected in incremental shells in the range

* To whom correspondence should be addressed at The Institute for Cancer Research.
† Present address: Department of Pharmacology, School of Medicine and Dentistry, University of Rochester, Rochester, NY 14642.
‡ Columbia University.

(1) (a) Barton, J. K.; Basile, L. A.; Danishefsky, A.; Alexandrescu, A. *Proc. Natl. Acad. Sci. U.S.A.* **1984**, *81*, 1961-1965. (b) Kumar, C.; Barton, J. K.; Turro, N. J. *J. Am. Chem. Soc.* **1985**, *107*, 5518-5523. (c) Barton, J. K.; Raphael, A. *J. Am. Chem. Soc.* **1984**, *106*, 2466-2468.
(2) Lin, C. T.; Bottcher, W.; Chou, M.; Creutz, C.; Sutin, N. *J. Am. Chem. Soc.* **1976**, *98*, 6536-6544.
(3) Takusagawa, F. Technical Report ICR-1982-0001-0001-01; The Institute for Cancer Research: Fox Chase, PA, 1982.

0020-1669/86/1325-0842$01.50/0 © 1986 American Chemical Society